

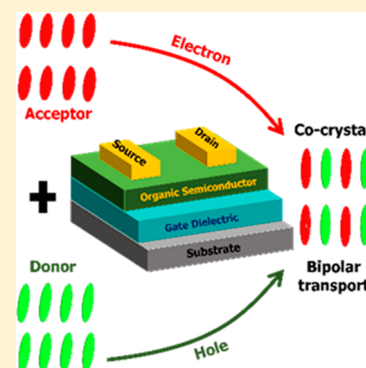
Theoretical Studies of Bipolar Transport in C_n BTBT– F_m TCNQ Donor–Acceptor Cocrystals

Qi Wei, Lei Liu, Shiyun Xiong,* Xiujuan Zhang, Wei Deng,[†] Xiaohong Zhang,[†] and Jiansheng Jie*[‡]

Institute of Functional Nano & Soft Materials (FUNSOM), Jiangsu Key Laboratory for Carbon-Based Functional Materials & Devices, Soochow University, 199 Ren'ai Road, Suzhou 215123, Jiangsu, P.R. China

Supporting Information

ABSTRACT: The development of crystals with bipolar transport characteristics is essential for high-performance organic field effect transistor (OFET) devices. In this work, we theoretically investigated the bipolar transport behaviors in C_n BTBT– F_m TCNQ cocrystals. It is found that bipolar transport can be realized in C_8 BTBT–TCNQ and C_{12} BTBT–TCNQ cocrystals with room-temperature electron/hole mobility up to 1.8/0.75 and 2.5/1.8 $\text{cm}^2 \text{V}^{-1} \text{s}^{-1}$, respectively. The comparable electron- and hole-transfer integrals between the nearest-neighbor molecule pairs as well as the small hole reorganization energy of the TCNQ molecule are responsible for the balanced electron and hole mobilities. Moreover, because of the π – π stacking between neighboring molecules, all cocrystals show strong anisotropic transport characteristic for both electron and hole transport with the mobility along the π – π stacking direction much larger than those along the other two directions. This work provides the possibility of high-performance OFET engineering and also enriches the OFET families with bipolar transport characteristics.



In the past decade, the organic field effect transistors (OFETs) have attracted widespread attention because of their low cost, easy fabrication, and natural abundance.^{1–3} With the extensive studies of OFETs, more and more small organic molecules with high performance have been developed as thin-film materials,⁴ such as 2,7-dioctyl[1]benzothieno[3,2-*b*][1]benzothiophene (C_8 -BTBT),^{5,6} 6,13-bis-(triisopropylsilyl) ethynyl pentacene (TIPS-P),⁷ fluorinated anthradithiophene 2,8-difluoro-5,11 bis(triethylsilyl) ethynyl anthradithiophene (diF-TES ADT),^{8–10} and so on. Among which, 2,7-dialkyl[1]benzothieno[3,2-*b*][1] benzothiophene (C_n -BTBT) has been frequently investigated because of its strong intermolecular interactions, which lead to the formation of highly ordered crystal films with high mobility. According to previous reports, C_n BTBT possesses good p-type transmission characteristics, and its properties can be engineered by the alkyl side-chain length. The increase of the alkyl chain can improve the solubility of the molecule while it can also adjust the molecular packing mode. However, when the alkyl chain is too long, it can create a bulky insulator layer between semiconducting π – π stacks, limiting the vertical transport and diluting the number of π -systems close to the channel interface.^{11–13} Therefore, in practice, C_8 BTBT molecules are mostly used for p-type OFET. With the off-center spin-coating method, the hole mobility of C_8 BTBT can reach up to 43 $\text{cm}^2 \text{V}^{-1} \text{s}^{-1}$.¹⁴ Although the performance of p-type organic small molecules has been well-developed, the development of n-type organic semiconductor materials lags far behind.¹⁵ The synthesis method of n-type organic crystals with high electron mobility, air stability, and high solubility is extremely limited, which greatly hinders the development of OFET-related

flexible electronic devices. At present, 7,7',8,8'- tetracyanoquinodimethane (TCNQ) and its derivative molecules have been often used as n-type dopants in experiments to make the device have electron transport characteristics.^{16,17} On the other hand, TCNQ itself has been predicted to be a good n-type molecule with the electron mobility of 1.6 $\text{cm}^2 \text{V}^{-1} \text{s}^{-1}$ at room temperature.¹⁸ To further increase the electron mobility of the TCNQ molecule, F atoms, which are strong electron-withdrawing atoms, were introduced into the molecule, forming F_m TCNQ ($m = 0, 2, 4$). The electron mobility of F_2 TCNQ is predicted up to 25 $\text{cm}^2 \text{V}^{-1} \text{s}^{-1}$ at 150 K, higher than that of the other two structures.¹⁹ However, because of the bad environmental stability, low mobility, high cost, and other factors, the overall development of n-type organic semiconductors still lags behind that of p-type crystals. Considering that n-type and bipolar organic semiconductors play an important role in bipolar transistors and complementary circuits, the development of new bipolar semiconductor materials with high performance is still a key focus of organic electronics.^{20,21} Injecting holes and electrons from the same electrode into a single semiconductor is a key point but difficult to realize in bipolar transport. To solve this problem, a single electrode material is usually used in combination with two different semiconductors, i.e., a donor–acceptor bonded cocrystal material. One of them has a corresponding highest occupied molecular orbital (HOMO)

Received: November 21, 2019

Accepted: December 23, 2019

Published: December 23, 2019

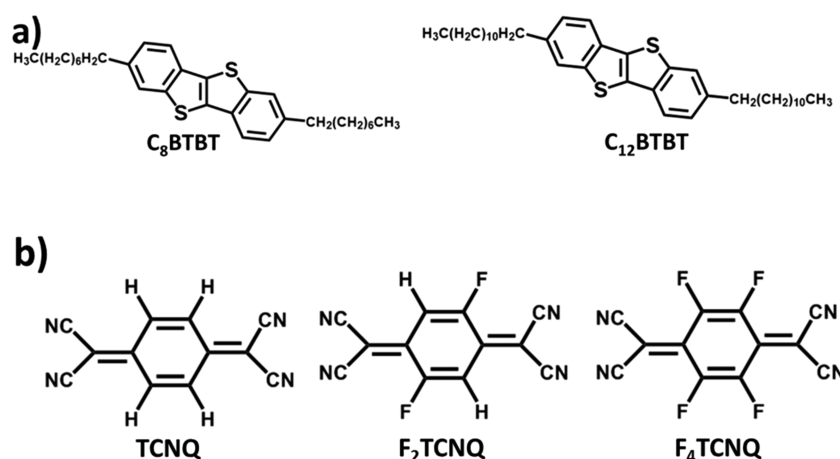


Figure 1. Molecule structures of (a) donor and (b) acceptor molecules.

energy level to transport holes, and the other has a suitable lowest unoccupied molecular orbital (LUMO) energy level for electron transport.²²

In this work, we studied the electron and hole transport behaviors of cocrystals composed of donor and acceptor molecules. We selected the typical p-type molecules C_8 BTBT and C_{12} BTBT and n-type molecules TCNQ, F_2 TCNQ, and F_4 TCNQ as donor (D) and acceptor (A) molecules, respectively. For cocrystal materials composed of donors and acceptors, there are two main stacking methods: ...DDD...AAA...²³ and ...DADADA...²⁴ Here we choose the structure with ...DADADA... stacking as schematically demonstrated in Figure S1, and the atomistic structures of each cocrystal are represented in Figure S2. According to the structure, the ratio between D and A is 1:1, and all six combination structures have been successfully synthesized experimentally.²⁵ The experimental lattice parameters are adopted in our studies. The full quantum band-like transport model²⁶ has been used for charge mobility simulations because of the small molecular mass in TCNQ.¹⁸ In fact, for cocrystal structures, the charge transport behavior is often manifested as a band-like transmission characteristic.²⁷

Experimental lattice structures are used in our studies. Table S1 illustrates the lattice information for structures with all D–A combinations.²⁸ The molecule structures of all donors and acceptors are shown in panels a and b of Figure 1, respectively. Because charges transport through the frontier orbitals, we first calculated the energy levels of all molecules. The obtained results are summarized in Figure 2, and the exact values are shown in Table S2. For C_8 BTBT and C_{12} BTBT, the frontier orbitals are almost unchanged, which is because the frontier orbitals are distributed on the BTBT part and the side chains have negligible effect on it (Figure S3). For TCNQ molecules, the substitution of H with F atoms can downshift both the HOMO and LUMO levels and the magnitude increases with the number of F atoms, which is due to the strong electron-withdrawing effect of F atoms. The energy gaps between the HOMO of donors and the LUMO of acceptors range from -0.12 to -0.37 eV. To realize bipolar transport, it is essential to have weak interactions between donor and acceptor molecules. To check that, we analyzed the Hirshfeld surfaces based on CrystalExplorer,²⁹ and the fingerprint is obtained for all cocrystals (Figure S4). According to the fingerprints, there exists π – π interaction between donor and acceptor molecules. In addition, hydrogen bonds like $N\cdots H$ and $S\cdots H$ can also be

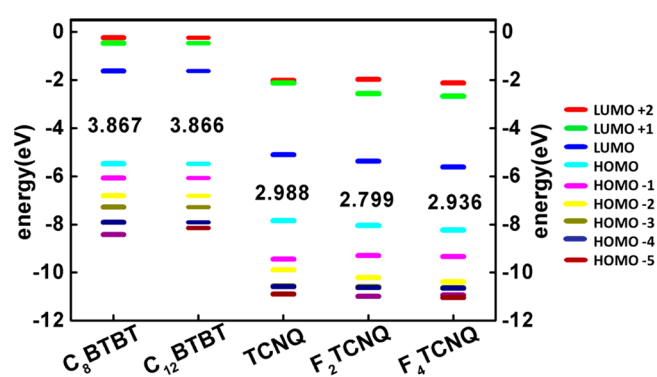


Figure 2. Energy levels of the acceptor and donor molecules with the HOMO–LUMO gaps indicated by the numbers.

found. The existence of the weak interaction can lead to charge transfer between donors and acceptors, which is favorable for bipolar transport.

The charge-transfer integral which is proportional to the hopping rates between two molecules characterizes the coupling strength between neighboring molecule pairs. There are multiple methods that can be used to calculate the transfer integral, including the energy level splitting method,³⁰ the finding energy level splitting minimum method,³¹ the lattice point energy correction method,³² and the direct coupling method.³³ The transfer integral is dependent on the relative angle of the dimer. When the relative angle is small, the four methods have certain accuracy.^{34,35} In our studied systems, all the dimer pairs are basically parallel and have central symmetry. For a cocrystal symmetrically stacked along a particular direction, the energy splitting method is widely use.³⁶ Therefore, in this work, we adopt the energy level splitting method to calculate the transfer integral. In all the structures, we calculated the transfer integral of all molecule pairs up to the third nearest neighbors with the F_m TCNQ molecule as the center. According to the molecule pair distances, there are three different transfer dimers in all structures, which we term T1, T2, and T3, which correspond to the nearest, the second-nearest, and the third-nearest neighbor pairs, respectively. Both T1 and T2 correspond to the molecular pair of C_n BTBT– F_m TCNQ, and T3 represents the molecular pair of F_m TCNQ– F_m TCNQ (Figure S5). The calculated transfer integral of T1, T2, and T3 is demonstrated in Figure 3. As shown in Figure 3a,b, for electron transport, the

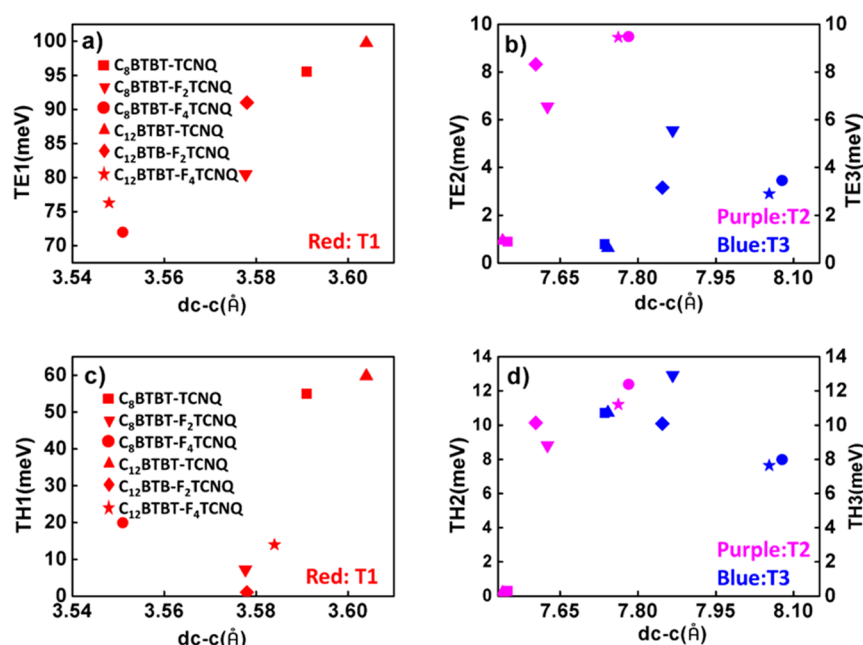


Figure 3. Electron- and hole-transfer integral for C_8 BTBT–TCNQ, C_8 BTBT– F_2 TCNQ, C_8 BTBT– F_4 TCNQ, C_{12} BTBT–TCNQ, C_{12} BTBT– F_2 TCNQ, and C_{12} BTBT– F_4 TCNQ cocrystals. (a) Electron-transfer integral for T1; (b) electron-transfer integral for T2 and T3; (c) hole-transfer integral for T1; (d) hole-transfer integral for T2 and T3. Panels b and d share the same notation shape as panels a and c.

Table 1. Reorganization Energy of the Studied Cocrystals

RE (meV)		C_8 BTBT–TCNQ	C_8 BTBT– F_2 TCNQ	C_8 BTBT– F_4 TCNQ	C_{12} BTBT–TCNQ	C_{12} BTBT– F_2 TCNQ	C_{12} BTBT– F_4 TCNQ
electron	C_n BTBT	317.81	318.90	314.42	308.80	313.80	319.28
	F_m TCNQ	260.62	235.93	235.80	260.97	235.41	236.67
hole	C_n BTBT	263.44	263.83	263.83	262.93	263.08	263.08
	F_m TCNQ	129.81	177.86	177.90	129.87	178.61	177.87

transfer integral of T1 is much larger than that of T2 and T3 because of relatively shorter distances. As a result, electrons jump most probably between adjacent molecules. The electron-transfer integral of T1 ranges from 71 to 100 meV for the six structures, and the value of C_{12} BTBT is larger than that of C_8 BTBT when the acceptor molecule is the same. For the C_8 BTBT donor, the electron-transfer integral of T1 decreases with the increase of the number of F atoms. For the C_{12} BTBT donor, the electron-transfer integral of T1 follows the trend F_2 TCNQ > TCNQ > F_4 TCNQ. For hole transport (Figure 3c,d), the transfer integrals of T1 for the six systems follow a broad distribution, ranging from 3.6 to 60 meV. For acceptors of F_4 TCNQ and F_2 TCNQ, the hole-transfer integral of T1 is relatively small, revealing a bad hole transport. However, in C_8 BTBT–TCNQ and C_{12} BTBT–TCNQ, their hole-transfer integral can reach 55 and 60 meV, respectively. The relatively large hole-transfer integral indicates that the two cocrystals may possess good hole mobility and can balance with their electron transport. Consequently, it is possibly to realize bipolar transport in these two systems.

The transfer integral characterizes the coupling between neighboring molecules; when a charge jumps from one molecule to another, the geometry of both molecules will change, leading to the change of corresponding energies. Such an energy change is defined as reorganization energy, and it plays an important role during charge transport. The reorganization energy during charge transfer can be divided into the internal and external parts. The external part which characterizes the environmental energy changes because the

charge transfer is much smaller than the internal one. As a result, it is usually ignored to simplify the calculations.³⁷ Table 1 summarizes the reorganization energy of donor and acceptor molecules for electron and hole transport. Interestingly, the reorganization energy of C_n BTBT is reduced only slightly when the side chain increases from 8 to 12 in all systems for both electron and hole transport, indicating that the side chains almost do not change their geometries during charge transport. For both C_8 BTBT and C_{12} BTBT, the reorganization energy is mostly contributed by the modes between 1500 and 1650 cm^{-1} for both electron and hole transport (Figure S6, panels a1–f1 and a3–f3). The mode with the maximum reorganization energy is around 1620 cm^{-1} for all cases, which corresponds to the symmetrical stretching vibration of the BTBT part. For F_m TCNQ, the reorganization energy of electrons decreases with the appearance of F atoms in both C_8 BTBT– F_m TCNQ and C_{12} BTBT– F_m TCNQ, whereas that for hole transport follows an opposite trend. Although the appearance of F atoms can change the reorganization energy of F_m TCNQ, the reorganization energy hardly changes when the number of F atoms increases from 2 to 4, possibly because of the equivalence of the four sites. Compared to the C_n BTBT molecule, the number of modes that contribute to the reorganization energy in F_m TCNQ is much less (Figure S6, panels a2–f2 and a4–f4), which eventually leads to smaller reorganization energies for F_m TCNQ in all systems for both electron and hole transport. The small reorganization energy for hole transport is also an advantage to balance the hole mobility and electron mobility, thus contributing to the

Table 2. Hopping Rates between Dimers in T1, T2, and T3

molecules		T1		T2		T3	
		hopping rates ($\times 10^{10} \text{ s}^{-1}$)	transfer integral (meV)	hopping rates ($\times 10^{10} \text{ s}^{-1}$)	transfer integral (meV)	hopping rates ($\times 10^{10} \text{ s}^{-1}$)	transfer integral (meV)
$\text{C}_8\text{BTBT}-\text{TCNQ}$	elec	0.10×10^5	95.56	0.93×10^0	0.91	0.68×10^0	0.78
	hole	0.39×10^4	54.92	0.12×10^0	0.30	0.15×10^3	10.71
$\text{C}_8\text{BTBT}-\text{F}_2\text{TCNQ}$	elec	0.72×10^4	80.56	0.48×10^2	6.55	0.34×10^2	5.56
	hole	0.67×10^2	7.17	1.00×10^2	8.82	0.21×10^3	12.92
$\text{C}_8\text{BTBT}-\text{F}_4\text{TCNQ}$	elec	0.61×10^4	71.97	0.11×10^3	9.52	0.14×10^2	3.45
	hole	0.51×10^3	19.86	0.20×10^3	12.38	0.82×10^2	7.98
$\text{C}_{12}\text{BTBT}-\text{TCNQ}$	elec	0.13×10^5	99.76	0.11×10^1	0.93	0.52×10^0	0.63
	hole	0.94×10^4	59.75	1.00×10^{-1}	0.20	0.30×10^3	10.74
$\text{C}_{12}\text{BTBT}-\text{F}_2\text{TCNQ}$	elec	0.14×10^5	91.02	0.12×10^3	8.33	0.17×10^2	3.16
	hole	0.20×10^1	1.04	0.19×10^3	10.13	0.19×10^3	10.09
$\text{C}_{12}\text{BTBT}-\text{F}_4\text{TCNQ}$	elec	0.63×10^4	76.30	0.97×10^3	9.48	0.91×10^1	2.90
	hole	0.25×10^3	13.94	0.16×10^3	11.21	0.76×10^2	7.64

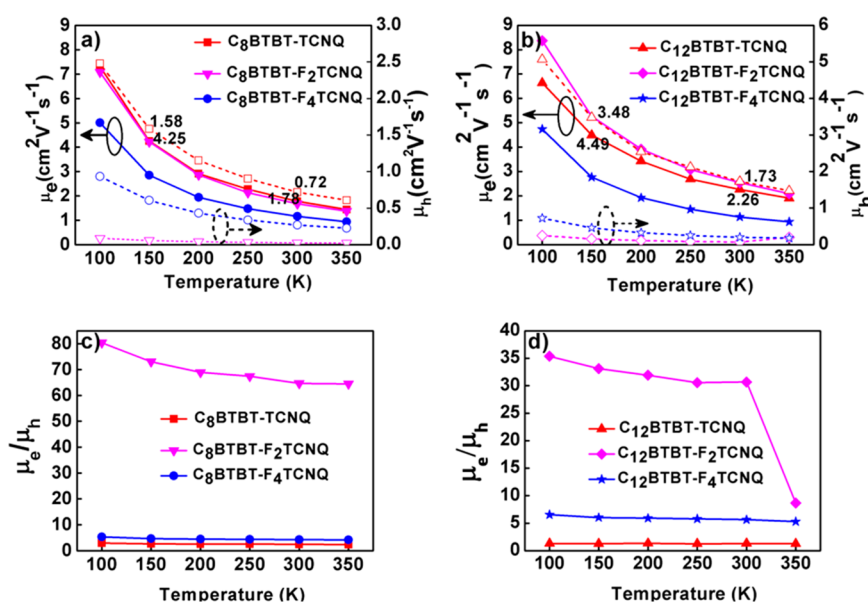


Figure 4. Electron and hole mobilities of $\text{C}_8\text{BTBT}-\text{F}_m\text{TCNQ}$ (a) and $\text{C}_{12}\text{BTBT}-\text{F}_m\text{TCNQ}$ (b) eutectic crystals as a function of temperature. The solid lines indicate the mobility of electrons, and the dotted lines indicate the mobility of holes. (c and d) Ratio between electron and hole mobilities for $\text{C}_8\text{BTBT}-\text{F}_m\text{TCNQ}$ (c) and $\text{C}_{12}\text{BTBT}-\text{F}_m\text{TCNQ}$ (d). The ratio μ_e/μ_h characterizes the balance between electron and hole transport.

realization of bipolar transport. The mode with the maximum reorganization energy in F_mTCNQ is always at 1500 cm^{-1} for all cases, corresponding to the stretching mode of vibration as illustrated by the inset images in Figure S6. From Figure S6, we can also find that the coupling between electrons and phonons is local in the F_mTCNQ molecule for the case of hole transport as only the modes beyond 1200 cm^{-1} contribute to the reorganization energy. For the other cases, both low and high frequencies have non-negligible contributions to the reorganization energies, indicating the interaction between electrons and phonons involves both local and nonlocal couplings.³⁸

On the basis of the energy levels, transfer integral, and reorganization energy, one can calculate the charge hopping rates between any molecule pairs. Table 2 illustrates the hopping rates between molecule pairs within the third nearest molecule neighbors for both electron and hole transport. In general, the hopping rates decrease with the increase of molecule pair distances except for the hole transport in $\text{C}_8\text{BTBT}-\text{F}_2\text{TCNQ}$ and $\text{C}_{12}\text{BTBT}-\text{F}_2\text{TCNQ}$. In these two cases, the hopping rates of T2 and T3 are larger than that of

T1 because of the larger transfer integral of T2 and T3. For T1, the electron hopping rates are larger than the hole ones in all cases, indicating that all those systems prefer to transport electrons. In $\text{C}_8\text{BTBT}-\text{TCNQ}$ and $\text{C}_{12}\text{BTBT}-\text{TCNQ}$, the difference between hole and electron hopping rates is the smallest, especially in $\text{C}_{12}\text{BTBT}-\text{TCNQ}$, where the hopping rate of hole transport is only slightly smaller than that of electron transport, which demonstrates that it is possible to realize bipolar transport in these two systems.

To quantitatively characterize the transport behavior of each system, we simulated the charge mobilities from 100 to 350 K based on the dynamic Monte Carlo random walk model. The corresponding results are demonstrated in Figure 4a,b. As the temperature increases, the mobility of both electrons and holes decreases gradually. In $\text{C}_8\text{BTBT}-\text{F}_m\text{TCNQ}$ systems, the electron mobility follows the trend $\text{TCNQ} \approx \text{F}_2\text{TCNQ} > \text{F}_4\text{TCNQ}$, while the hole mobility follows the trend $\text{TCNQ} > \text{F}_4\text{TCNQ} > \text{F}_2\text{TCNQ}$. In the three systems, $\text{C}_8\text{BTBT}-\text{TCNQ}$ possesses the largest electron and hole mobilities; the corresponding values at 300 K are 1.78 and $0.72 \text{ cm}^2 \text{ V}^{-1}$

s^{-1} , respectively. The ratio between electron and hole mobility is ~ 3 , which also corresponds to the best balanced value among the three eutectic crystals, as shown in Figure 4c,d. Although $\text{C}_8\text{BTBT}-\text{F}_2\text{TCNQ}$ also demonstrates high electron mobility, it is not a good hole transport material and thus can not realize the bipolar transport. In $\text{C}_{12}\text{BTBT}-\text{F}_m\text{TCNQ}$, the electron mobility in the whole temperature range follows the trend $\text{F}_2\text{TCNQ} > \text{TCNQ} > \text{F}_4\text{TCNQ}$ and the trend of hole mobility follows $\text{TCNQ} > \text{F}_4\text{TCNQ} > \text{F}_2\text{TCNQ}$. In the three systems, $\text{C}_{12}\text{BTBT}-\text{TCNQ}$ shows the best balanced electron and hole transport behavior with the ratio between electron and hole mobility of ~ 1.4 . The corresponding electron and hole mobility can reach 2.26 and $1.73 \text{ cm}^2 \text{ V}^{-1} \text{ s}^{-1}$ at room temperature, respectively. Therefore, in all 6 eutectic systems, only the combinations of TCNQ with $\text{C}_8\text{BTBT}/\text{C}_{12}\text{BTBT}$ can realize bipolar transport. The combinations with F_2TCNQ or F_4TCNQ can be used only as n-type transport materials because of the strong electron-withdrawing ability of F atoms. The increase of side-chain length in $\text{C}_n\text{BTBT}-\text{TCNQ}$ can enhance the hole mobility, thus further improving the bipolar transport in our studied systems. Because the energy levels do not change with the side-chain length as discussed before, the enhanced hole mobility should originate from different stacking modes of different structures. Actually, the degree of π conjugation in the yz plane of C_{12} systems is greater than that of C_8 systems (Figure S7), which may eventually improve the hole mobilities in C_{12} systems. On the basis of the above analysis, we successfully realized the bipolar transport in $\text{C}_8\text{BTBT}/\text{C}_{12}\text{BTBT}-\text{TCNQ}$ through eutectic design with electron and hole transport components.

To gain deeper knowledge regarding the transport characteristics of all structures, we calculated the mobility of the six structures along the three lattice directions at 300 K. As demonstrated in Figure 5a–d, all systems show large

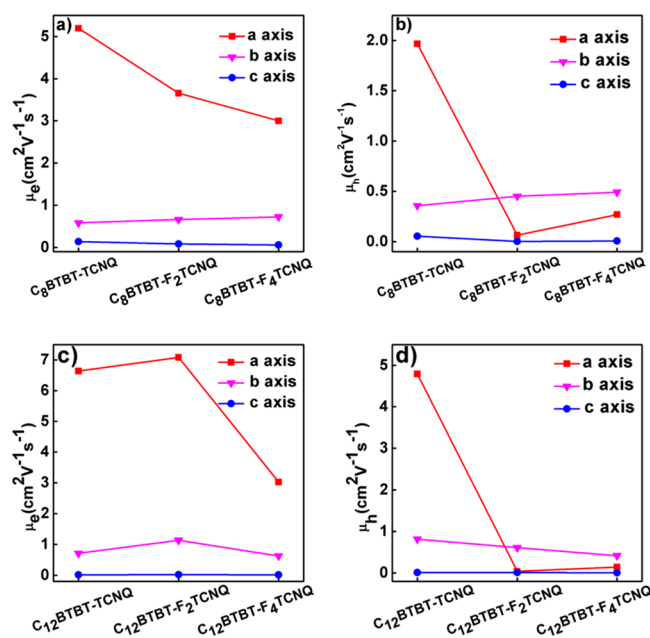


Figure 5. Crystal direction-dependent electron and hole mobilities of $\text{C}_8\text{BTBT}-\text{F}_m\text{TCNQ}$ and $\text{C}_{12}\text{BTBT}-\text{F}_m\text{TCNQ}$ at 300 K: (a) electron mobility for $\text{C}_8\text{BTBT}-\text{F}_m\text{TCNQ}$, (b) hole mobility for $\text{C}_8\text{BTBT}-\text{F}_m\text{TCNQ}$, (c) electron mobility for $\text{C}_{12}\text{BTBT}-\text{F}_m\text{TCNQ}$, and (d) hole mobility for $\text{C}_{12}\text{BTBT}-\text{F}_m\text{TCNQ}$.

anisotropic electron and hole transport characteristics. In all systems, as the interaction between molecules along the c crystal orientation is very weak, they show very small mobilities along the c -direction for both electrons and holes. Actually, all T1, T2, and T3 are almost in the a – b lattice plane and thus do not contribute to the transport in the c -direction. For electron transport, the mobility along the a -direction is the largest for all systems. This is because the direction of T1 is close to the a -direction, and T2/T3 is close to the b -direction, and the transfer integral of T1 for electron transport is much larger than that of T2 and T3. For hole transport, the mobility is still the largest along the a -direction in $\text{C}_n\text{BTBT}-\text{TCNQ}$ while it changes to the b -direction in the other four systems. In $\text{C}_n\text{BTBT}-\text{F}_2\text{TCNQ}$ and $\text{C}_n\text{BTBT}-\text{F}_4\text{TCNQ}$, the transfer integral of T2 and/or T3 is larger or comparable to that of T1 for hole transport. Together with the larger distances of T2 and T3, it eventually leads to the maximum mobility along the b -direction. The large anisotropic transport behavior in those systems offers the opportunity to design devices with high mobilities.³⁹ For example, if we adopt $\text{C}_{12}\text{BTBT}-\text{TCNQ}$ to design a device with the transport along the a -direction, we can obtain bipolar transport with electron and hole mobilities as high as 6.6 and $4.9 \text{ cm}^2 \text{ V}^{-1} \text{ s}^{-1}$, respectively. It is worth mentioning that our simulated mobilities correspond to the value of perfect lattices. In real experiments, the value may be lower than our simulated results because of the existence of defects. However, the trends among different molecules predicted by our simulations, especially the bipolar transport characteristics, are still meaningful to guide experiments.

In this work, the hole and electron transport behaviors in $\text{C}_n\text{BTBT}-\text{F}_m\text{TCNQ}$ ($n = 8$ and 12 and $m = 0, 2$, and 4) cocrystals are studied based on the KMC and DFT calculations. C_nBTBT and F_mTCNQ molecules serve as electron donor and acceptor, respectively, because of the relatively higher HOMO level of C_nBTBT compared to that of F_mTCNQ . Among all 6 cocrystals, $\text{C}_n\text{BTBT}-\text{F}_2\text{TCNQ}$ shows the largest electron mobility while their hole mobility is very small because of the big differences of transfer integrals, which eventually leads to unbalanced electron and hole transport. However, $\text{C}_8\text{BTBT}-\text{TCNQ}$ and $\text{C}_{12}\text{BTBT}-\text{TCNQ}$ cocrystals can transport both electrons and holes with large mobilities, showing the bipolar transport characteristics. The room-temperature electron/hole mobility can reach up to $1.8/0.75$ and $2.5/1.8 \text{ cm}^2 \text{ V}^{-1} \text{ s}^{-1}$ for $\text{C}_8\text{BTBT}-\text{TCNQ}$ and $\text{C}_{12}\text{BTBT}-\text{TCNQ}$, respectively. The bipolar transport character in $\text{C}_n\text{BTBT}-\text{TCNQ}$ arises from two aspects: the comparable electron- and hole-transfer integral between the nearest neighbor molecule pairs and the smaller hole reorganization energy of the TCNQ molecule. In $\text{C}_n\text{BTBT}-\text{F}_4\text{TCNQ}$ systems, although the transfer integral of electrons between the nearest neighbor molecular pairs is 1 order of magnitude larger than that of holes, the transfer integral between second nearest neighbors for hole transport is comparable to the value of the nearest neighbors, which leads to enhanced hole mobility and improved bipolar transportation compared to $\text{C}_n\text{BTBT}-\text{F}_2\text{TCNQ}$. Because of the π – π stacking nature of the structures, all cocrystals show large anisotropic transport behavior with the mobility along the π – π stacking direction much larger than those along the other two directions. Such big anisotropic transport features could be useful for the design of high-performance organic devices with single-direction transport.

■ COMPUTATIONAL METHODS

All the DFT calculations are performed with Gaussian 09⁴⁰ at the B3LYP/6-311G level of theory. For mobility calculations, we have adopted the kinetic Monte Carlo (KMC) method implemented in MOMAP.⁴¹ The hopping rates between molecules are calculated with the nuclear tunneling model.³⁷ For KMC simulations, we used an $8 \times 8 \times 3$ supercell in the crystallographic *a*, *b*, and *c* directions, respectively. The transfer integral is evaluated up to the third nearest neighbors.

■ ASSOCIATED CONTENT

Supporting Information

The Supporting Information is available free of charge at <https://pubs.acs.org/doi/10.1021/acs.jpclett.9b03439>.

Atomistic structure of cocrystals; frontier orbital (HOMO and LUMO) distribution of the donor (C₈BTBT and C₁₂BTBT) and acceptor (TCNQ, F₂TCNQ, and F₄TCNQ) molecules; weak interactions within each crystal based on the Hirshfeld analysis; schematic illustration of the nearest-neighbor (T1), the second (T2), and the third nearest-neighbor (T3) molecular pairs in all systems; frequency-resolved reorganization energies and the vibration mode corresponding to the frequency with maximum reorganization energy (PDF)

■ AUTHOR INFORMATION

Corresponding Authors

*E-mail: syxiong@suda.edu.cn.

*E-mail: jsjie@suda.edu.cn.

ORCID

Wei Deng: 0000-0002-0067-0624

Xiaohong Zhang: 0000-0002-6732-2499

Jiansheng Jie: 0000-0002-2230-4289

Notes

The authors declare no competing financial interest.

■ ACKNOWLEDGMENTS

This work is supported by the National Natural Science Foundation of China (Nos. 51821002, 11804242, 91833303, 51672180, 51622306, and 21673151), the Natural Science Foundation of Jiangsu Province of China (BK20180845), Collaborative Innovation Center of Suzhou Nano Science & Technology (Nano-CIC), the Priority Academic Program Development of Jiangsu Higher Education Institutions (PAPD), the 111 Project, and Joint International Research Laboratory of Carbon-Based Functional Materials and Devices.

■ REFERENCES

- (1) Zhang, Y.; Jie, J.; Sun, Y.; Jeon, S. G.; Zhang, X.; Dai, G.; Lee, C. J.; Zhang, X. Precise Patterning of Organic Single Crystals via Capillary-Assisted Alternating-Electric Field. *Small* **2017**, *13*, 1604261.
- (2) Zhang, X.; Jie, J.; Deng, W.; Shang, Q.; Wang, J.; Wang, H.; Chen, X.; Zhang, X. Alignment and Patterning of Ordered Small-Molecule Organic Semiconductor Micro-/Nanocrystals for Device Applications. *Adv. Mater.* **2016**, *28*, 2475–2503.
- (3) Deng, W.; Zhang, X.; Wang, L.; Wang, J.; Shang, Q.; Zhang, X.; Huang, L.; Jie, J. Wafer-Scale Precise Patterning of Organic Single-Crystal Nanowire Arrays via a Photolithography-Assisted Spin-Coating Method. *Adv. Mater.* **2015**, *27*, 7305–7312.
- (4) Zhang, X.; Deng, W.; Jia, R.; Zhang, X.; Jie, J. Precise Patterning of Organic Semiconductor Crystals for Integrated Device Applications. *Small* **2019**, *15*, 1900332.
- (5) Chai, Z.; Abbasi, S. A.; Busnaina, A. A. Scalable Directed Assembly of Highly Crystalline 2,7-Dioctyl[1]benzothieno[3,2-*b*] [1]benzothiophene (C₈-BTBT) Films. *ACS Appl. Mater. Interfaces* **2018**, *10*, 18123–18130.
- (6) Zhao, W.; Jie, J.; Wei, Q.; Lu, Z.; Jia, R.; Deng, W.; Zhang, X.; Zhang, X. A Facile Method for the Growth of Organic Semiconductor Single Crystal Arrays on Polymer Dielectric toward Flexible Field-Effect Transistors. *Adv. Funct. Mater.* **2019**, *29*, 1902494.
- (7) Giri, G.; Verploegen, E.; Mannsfeld, S. C.; Atahan-Evrenk, S.; Kim, D. H.; Lee, S. Y.; Becerril, H. A.; Aspuru-Guzik, A.; Toney, M. F.; Bao, Z. Tuning charge transport in solution-sheared organic semiconductors using lattice strain. *Nature* **2011**, *480*, 504.
- (8) Rubinger, C. P. L.; Haneef, H. F.; Hewitt, C.; Carroll, D.; Anthony, J. E.; Jurchescu, O. D. Influence of solvent additives on the morphology and electrical properties of diF-TES ADT organic field-effect transistors. *Org. Electron.* **2019**, *68*, 205–211.
- (9) Deng, W.; Lu, B.; Mao, J.; Lu, Z. J.; Zhang, X. J.; Jie, J. Precise Positioning of Organic Semiconductor Single Crystals with Two-Component Aligned Structure through 3D Wettability-Induced Sequential Assembly. *ACS Appl. Mater. Interfaces* **2019**, *11*, 36205–36212.
- (10) Deng, W.; Zhang, X. J.; Jia, R.; Huang, L.; Zhang, X. H.; Jie, J. Organic molecular crystal-based photosynaptic devices for an artificial visual-perception system. *NPG Asia Mater.* **2019**, *11*, 77.
- (11) Dong, H.; Fu, X.; Liu, J.; Wang, Z.; Hu, W. 25th anniversary article: key points for high-mobility organic field-effect transistors. *Adv. Mater.* **2013**, *25*, 6158–6183.
- (12) Amin, A. Y.; Khassanov, A.; Reuter, K.; Meyer-Friedrichsen, T.; Halik, M. Low-voltage organic field effect transistors with a 2-tridecyl[1]benzothieno[3,2-*b*][1]benzothiophene semiconductor layer. *J. Am. Chem. Soc.* **2012**, *134*, 16548–16550.
- (13) Meng, H.; Zheng, J.; Lovinger, A. J.; Wang, B. C.; Van Patten, P. G.; Bao, Z. Oligofluorene-Thiophene Derivatives as High-Performance Semiconductors for Organic Thin Film Transistors. *Chem. Mater.* **2003**, *15*, 1778–1787.
- (14) Yuan, Y.; Giri, G.; Ayzner, A. L.; Zoombelt, A. P.; Mannsfeld, S. C.; Chen, J.; Nordlund, D.; Toney, M. F.; Huang, J.; Bao, Z. Ultra-high mobility transparent organic thin film transistors grown by an off-centre spin-coating method. *Nat. Commun.* **2014**, *5*, 3005.
- (15) Wang, L.; Zhang, X.; Dai, G.; Deng, W.; Jie, J.; Zhang, X. High-mobility air-stable n-type field-effect transistors based on large-area solution-processed organic single-crystal arrays. *Nano Res.* **2018**, *11*, 882–891.
- (16) Goldmann, M.; Hassan, A. K.; Basova, T.; Gürek, A. G.; Ahsen, V.; Guenoun, P. Anthracene and TCNQ doping of substituted nickel phthalocyanine: Effects on the electrical and optical properties of spin coated thin films. *MATEC Web Conf.* **2013**, *4*, 01002.
- (17) Mendez, H.; Heime, G.; Winkler, S.; Frisch, J.; Opitz, A.; Sauer, K.; Wegner, B.; Oehzelt, M.; Rothel, C.; Duham, S.; Tobben, D.; Koch, N.; Salzmann, I. Charge-transfer crystallites as molecular electrical dopants. *Nat. Commun.* **2015**, *6*, 8560.
- (18) Menard, E.; Podzorov, V.; Hur, S. H.; Gaur, A.; Gershenson, M. E.; Rogers, J. A. High-Performance n- and p-Type Single-Crystal Organic Transistors with Free-Space Gate Dielectrics. *Adv. Mater.* **2004**, *16*, 2097–2101.
- (19) Krupskaya, Y.; Gibertini, M.; Marzari, N.; Morpurgo, A. F. Band-like electron transport with record-high mobility in the TCNQ family. *Adv. Mater.* **2015**, *27*, 2453–2458.
- (20) Zhao, Y.; Guo, Y.; Liu, Y. 25th anniversary article: recent advances in n-type and ambipolar organic field-effect transistors. *Adv. Mater.* **2013**, *25*, 5372–5391.
- (21) Zhang, X.; Mao, J.; Deng, W.; Xu, X.; Huang, L.; Zhang, X.; Lee, S. T.; Jie, J. Precise Patterning of Laterally Stacked Organic Microbelt Heterojunction Arrays by Surface-Energy-Controlled Stepwise Crystallization for Ambipolar Organic Field-Effect Transistors. *Adv. Mater.* **2018**, *30*, 1800187.

- (22) Meijer, E. J.; de Leeuw, D. M.; Setayesh, S.; van Veenendaal, E.; Huisman, B. H.; Blom, P. W.; Hummelen, J. C.; Scherf, U.; Kadam, J.; Klapwijk, T. M. Solution-processed ambipolar organic field-effect transistors and inverters. *Nat. Mater.* **2003**, *2*, 678–682.
- (23) Hu, P.; Du, K.; Wei, F.; Jiang, H.; Kloc, C. Crystal Growth, HOMO–LUMO Engineering, and Charge Transfer Degree in Perylene-FxTCNQ ($x = 1, 2, 4$) Organic Charge Transfer Binary Compounds. *Cryst. Growth Des.* **2016**, *16*, 3019–3027.
- (24) Iijima, K.; Sanada, R.; Yoo, D.; Sato, R.; Kawamoto, T.; Mori, T. Carrier Charge Polarity in Mixed-Stack Charge-Transfer Crystals Containing Dithienobenzodithiophene. *ACS Appl. Mater. Interfaces* **2018**, *10*, 10262–10269.
- (25) Zhu, L.; Geng, H.; Yi, Y.; Wei, Z. Charge transport in organic donor-acceptor mixed-stack crystals: the role of nonlocal electron-phonon couplings. *Phys. Chem. Chem. Phys.* **2017**, *19*, 4418–4425.
- (26) Lin, L.; Fan, J.; Jiang, S.; Wang, Z.; Wang, C. K. Temperature dependence of electron mobility in N-type organic molecular crystals: Theoretical study. *Chem. Phys. Lett.* **2017**, *688*, 19–25.
- (27) Shimada, T.; Takahashi, Y.; Harada, J.; Hasegawa, H.; Inabe, T. Band-Like Carrier Transport at the Single-Crystal Contact Interfaces between 2,5-Difluoro-7,7,8,8-tetracyanoquinodimethane and Electron Donors. *J. Phys. Chem. Lett.* **2018**, *9*, 420–424.
- (28) Tsutsumi, J. Y.; Matsuoka, S.; Inoue, S.; Minemawari, H.; Yamada, T.; Hasegawa, T. N-type field-effect transistors based on layered crystalline donor–acceptor semiconductors with dialkylated benzothienobenzothiophenes as electron donors. *J. Mater. Chem. C* **2015**, *3*, 1976–1981.
- (29) Turner, M.; McKinnon, J.; Wolff, S.; Grimwood, D.; Spackman, P.; Jayatilaka, D.; Spackman, M. *CrystalExplorer17*; University of Western Australia Crawley: Western Australia, Australia, 2017.
- (30) Brédas, J. L.; Beljonne, D.; Coropceanu, V.; Cornil, J. M. Charge-Transfer and Energy-Transfer Processes in π -Conjugated Oligomers and Polymers: A Molecular Picture. *Chem. Rev.* **2004**, *104*, 4971–5004.
- (31) Li, X. Y. Electron transfer between tryptophan and tyrosine: Theoretical calculation of electron transfer matrix element for intramolecular hole transfer. *J. Comput. Chem.* **2001**, *22*, 565–579.
- (32) Zhu, L.; Geng, H.; Yi, Y.; Wei, Z. Charge transport in organic donor–acceptor mixed-stack crystals: the role of nonlocal electron–phonon couplings. *Phys. Chem. Chem. Phys.* **2017**, *19*, 4418–4425.
- (33) Hu, P.; Li, H.; Li, Y.; Jiang, H.; Kloc, C. Single-crystal growth, structures, charge transfer and transport properties of anthracene-F₄TCNQ and tetracene-F₄TCNQ charge-transfer compounds. *CrystEngComm* **2017**, *19*, 618–624.
- (34) Valeev, E. F.; Coropceanu, V.; da Silva Filho, D. A.; Salman, S.; Brédas, J. L. Effect of electronic polarization on charge-transport parameters in molecular organic semiconductors. *J. Am. Chem. Soc.* **2006**, *128*, 9882–9886.
- (35) Yang, X.; Li, Q.; Shuai, Z. Theoretical modelling of carrier transports in molecular semiconductors: molecular design of triphenylamine dimer systems. *Nanotechnology* **2007**, *18*, 424029.
- (36) Zhang, J.; Gu, P.; Long, G.; Ganguly, R.; Li, Y.; Aratani, N.; Yamada, H.; Zhang, Q. Switching charge-transfer characteristics from p-type to n-type through molecular “doping” (co-crystallization). *Chem. Sci.* **2016**, *7*, 3851–3856.
- (37) Nan, G.; Yang, X.; Wang, L.; Shuai, Z.; Zhao, Y. Nuclear tunneling effects of charge transport in rubrene, tetracene, and pentacene. *Phys. Rev. B: Condens. Matter Mater. Phys.* **2009**, *79*, 115203.
- (38) Sosorev, A. Y.; Maslennikov, D. R.; Chernyshov, I. Y.; Dominskiy, D. I.; Bruevich, V. V.; Vener, M. V.; Parashuk, D. Y. Relationship between electron–phonon interaction and low-frequency Raman anisotropy in high-mobility organic semiconductors. *Phys. Chem. Chem. Phys.* **2018**, *20*, 18912–18918.
- (39) Deng, W.; Zhang, X.; Dong, H.; Jie, J.; Xu, X.; Liu, J.; He, L.; Xu, L.; Hu, W.; Zhang, X. Channel-restricted meniscus self-assembly for uniformly aligned growth of single-crystal arrays of organic semiconductors. *Mater. Today* **2019**, *24*, 17–25.
- (40) Fircchk, M.; Trucks, G.; Schlegel, H.; Scuseria, G.; Robb, M.; Cheeseman, J.; Scalmani, G.; Barone, V.; Mennucci, B.; Petersson, G. A. *Gaussian 09*, revision D01; Gaussian, Inc.: Wallingford, CT, 2009.
- (41) Niu, Y.; Li, W.; Peng, Q.; Geng, H.; Yi, Y.; Wang, L.; Nan, G.; Wang, D.; Shuai, Z. MOlecular MAterials Property Prediction Package (MOMAP) 1.0: a software package for predicting the luminescent properties and mobility of organic functional materials. *Mol. Phys.* **2018**, *116*, 1078–1090.